Radiation Protection Dosimetry (2016), Vol. 168, No. 2, pp. 154–166 doi:10.1093/rpd/ncv181
Advance Access publication 21 April 2015

BUBBLE-DETECTOR MEASUREMENTS OF NEUTRON RADIATION IN THE INTERNATIONAL SPACE STATION: ISS-34 TO ISS-37

M. B. Smith[1,*], S. Khulapko[2,3], H. R. Andrews[1], V. Arkhangelsky[2], H. Ing[1], M. R. Koslowksy[1], B. J. Lewis[4], R. Machrafi[4], I. Nikolaev[3] and V. Shurshakov[2]
[1]Bubble Technology Industries, PO Box 100, Chalk River, ON, Canada K0J 1J0
[2]Institute for Biomedical Problems, Russian Academy of Sciences, 76A Khoroshevskoe sh., Moscow 123007, Russia
[3]RSC-Energia, 4A Lenin str., Korolev, Moscow Region 141070, Russia
[4]Faculty of Energy Systems and Nuclear Science, University of Ontario Institute of Technology, 2000 Simcoe Street North, Oshawa, ON, Canada L1H 7K4

*Corresponding author: smithm@bubbletech.ca

Received 29 August 2014; revised 2 March 2015; accepted 6 March 2015

Bubble detectors have been used to characterise the neutron dose and energy spectrum in several modules of the International Space Station (ISS) as part of an ongoing radiation survey. A series of experiments was performed during the ISS-34, ISS-35, ISS-36 and ISS-37 missions between December 2012 and October 2013. The Radi-N2 experiment, a repeat of the 2009 Radi-N investigation, included measurements in four modules of the US orbital segment: Columbus, the Japanese experiment module, the US laboratory and Node 2. The Radi-N2 dose and spectral measurements are not significantly different from the Radi-N results collected in the same ISS locations, despite the large difference in solar activity between 2009 and 2013. Parallel experiments using a second set of detectors in the Russian segment of the ISS included the first characterisation of the neutron spectrum inside the tissue-equivalent Matroshka-R phantom. These data suggest that the dose inside the phantom is ∼70 % of the dose at its surface, while the spectrum inside the phantom contains a larger fraction of high-energy neutrons than the spectrum outside the phantom. The phantom results are supported by Monte Carlo simulations that provide good agreement with the empirical data.

INTRODUCTION

The bubble detector[1–5] has been used to monitor neutron radiation in space since 1989. Early experiments on recoverable Russian Biocosmos (Bion) satellites, the Mir space station and the space shuttle provided important information on the neutron dose inside the various spacecraft[3, 4]. While these early measurements were sporadic, the frequency of bubble-detector measurements in low-Earth orbit (LEO) increased considerably following the advent of the International Space Station (ISS). Experiments started in 2006 as part of the international Matroshka-R experiment based in the Russian segment of the ISS. Several measurements, each approximately a week long, were performed in the various Russian modules during the ISS-13 to ISS-19 missions[6, 7]. This included experiments with the Matroshka-R tissue-equivalent spherical phantom, which demonstrated that the dose received inside the phantom is lower than that at the phantom surface. These measurements were the first to use a special bubble detector, known as the space personal neutron dosemeter (SPND), developed specifically for space applications. A mini reader, designed and engineered for the ISS, was used for automatic read-out of the bubble data.

The Matroshka-R experiments with bubble detectors continued during the ISS-20 and ISS-21 missions in 2009[7]. At the same time, the Radi-N experiment commenced in the US Orbital Segment (USOS) of the ISS. The ISS-20/21 experiments were the first to use the space bubble-detector spectrometer (SBDS), a set of six detectors with different energy thresholds that is used to measure the neutron energy spectrum. A SBDS and two SPNDs were used to conduct week-long measurements in each of the Russian service module, Columbus, the US laboratory and the Japanese experiment module (JEM). With the limited counting statistics of the measurements, it was shown that the neutron spectrum was not strongly dependent on the exact location within the ISS.

Further bubble-detector measurements were performed for Matroshka-R during the ISS-22 (2009) to ISS-33 (2012) expeditions[8]. Thirty-two experimental sessions (∼1 week each) were performed in the Russian segment, using SPNDs and a SBDS. Some of the experiments were conducted using a hydrogenous radiation shield and a reduction in neutron dose was determined due to the shielding. This result was similar to that from an earlier bubble-detector experiment[7] in the JEM using a different water shield. The

bubble-detector data from 2009 to 2012 were compared with data from the ISS tissue-equivalent proportional counter (TEPC) and the Russian DB-8 dosemeters, which were co-located with the bubble detectors in the Russian segment at the time of the measurements. This inter-comparison agreed with previous empirical measurements[7, 9] and theoretical calculations[10], suggesting that neutrons account for ~30 % of the total dose equivalent in LEO. The 2009–12 data were also correlated with quantities that might be expected to influence the measurements, including the ISS altitude and solar activity. Surprisingly, it was demonstrated that altitude and solar activity did not seem to strongly affect the neutron dose or energy spectrum inside the ISS.

This article reports on experiments conducted between December 2012 and October 2013 during the ISS-34, ISS-35, ISS-36 and ISS-37 expeditions. These measurements continue the ongoing survey of neutron radiation in the ISS, adding to the data collected during ISS-13 to ISS-33. In the USOS, the Radi-N2 experiment started, with the goal of repeating the Radi-N measurements as closely as possible. Following the 2009 Radi-N experiments, it became clear that a single week-long measurement in each location (which suffers from relatively poor counting statistics) was insufficient to accurately assess potential differences in the neutron field in each ISS module. Consequently, Radi-N2 aims to add data from multiple sessions in each location to elucidate the nature of the neutron radiation in each module. As an initial step towards this goal, several experiments were performed in four USOS modules—Columbus, the US laboratory, the JEM and Node 2—during ISS-34 to ISS-36. The first three modules were also used for the Radi-N experiments, while the latter location was added for Radi-N2. In the Russian segment, experiments continued in the service module in order to improve the counting statistics for this location. Furthermore, the first spectroscopic measurements inside and around the Matroshka-R phantom were conducted during ISS-35/36 and the first two sessions of ISS-37/38. This activity was performed in the Russian mini research module 1 (MRM1), a location previously unexplored using bubble detectors.

MEASUREMENTS ON THE ISS

Bubble detector calibration

The detectors used in this work were calibrated at the Bubble Technology Industries facility using established procedures[7] developed for commercial bubble detectors. The detector sensitivity was calibrated using an AmBe source with a neutron emission rate of 1.13×10^7 s^{-1} and a conversion coefficient of 4.11×10^{-4} μSv cm^2 [according to the International Commission on Radiation Units and Measurements (ICRU) Report 66]. For SPNDs, the convention used for earlier bubble-detector measurements in space[5–8, 11, 12] was followed, whereby the detector sensitivity determined with the AmBe source is scaled by a factor of 1.62. This scaling factor accounts for the difference between the AmBe energy spectrum and the spectrum expected in space. It was determined using theoretical calculations of the bubble-detector response and measurements that validated these calculations[5, 11, 12]. Following this procedure, the dosimetric quantity reported by bubble detectors in the space environment is the ambient dose equivalent, $H^*(10)$. For the SBDS, a measured response matrix[7] is used to unfold the data. The spectrum bins used by the unfolding algorithm cover six energy ranges: 0.06–0.25; 0.25–0.6; 0.6–2; 2–3.5; 3.5–15 and 15–50 MeV. The use of an empirical response matrix makes adjustment of the AmBe calibration unnecessary for the SBDS. It should be noted that neutrons with energies higher than 50 MeV are included in the highest energy bin of the SBDS spectrum. The response of the bubble detector to high-energy neutrons is discussed in Smith *et al.*[7, 13].

Two sets of bubble detectors were delivered to the ISS at the start of ISS-34, each set consisting of a SBDS and two SPNDs. The detectors were of the same type used for the earlier ISS experiments during ISS-13 to ISS-33[6–8]. The characteristics of the four SPNDs used in this work are provided in Table 1, and the properties of the 12 SBDS detectors are presented in Table 2. The sensitivity of the SPNDs is provided from both the AmBe calibration (S_{AmBe}) and after conversion for use in space (S). For the SBDS, the detector type and AmBe sensitivity (S_{AmBe}) are given.

Dates and locations

The measurements described in this article cover the period from December 2012 (ISS-34) to October 2013 (ISS-37). Thirteen pairs of concurrent sessions were performed (i.e. a total of 26 sessions) with each session being approximately 1 week long. Dates and detector locations for the experimental sessions are provided in Table 3. For each session, labelled as A–M, the locations of the SBDS from detector set 1 (detectors A91–A96) and the SBDS from set 2 (A01–A06) are provided.

Table 1. Characteristics of the SPNDs used in this work.

Detector set	Detector number	Serial number	S_{AmBe} (bubble mSv^{-1})	S (bubble mSv^{-1})
1	A97	2515	148 ± 24	91 ± 15
1	A98	2615	146 ± 16	90 ± 10
2	A07	2717	167 ± 18	103 ± 11
2	A08	2417	165 ± 21	102 ± 13

The SBDS locations for the Radi-N2 measurements were Columbus, panel COL1A3; the US laboratory, panel 1S4; the JEM, panel FD3/JPM1F3; and Node 2, panel P3. (A panel is a section of the interior wall of the ISS with a specific label.) These locations refer to the SBDS from detector set 1. Two SPNDs (A97 and A98, also part of set 1) were deployed simultaneously with the SBDS measurements. For sessions A–D, one SPND was placed in an astronaut's sleeping quarters in Node 2, while the second detector was worn on his body. This procedure enables a comparison of the neutron dose in the sleeping quarters to an average from around the ISS and was also performed as part of the Radi-N experiment during ISS-20/21. For the later Radi-N2 sessions (G, H, J and K), the two SPNDs were co-located with the SBDS.

In the Russian segment, the measurement locations were the service module and MRM1. While the service module has been well studied in earlier Matroshka-R measurements, MRM1 provided the opportunity to perform experiments in a new location. In the service module, the location for the SBDS and two SPNDs from detector set 2 was panel 327, with the exception of session C. For this session, the SBDS and SPNDs were placed on and around the hydrogenous radiation shield[8] in the service module. The Matroshka-R spherical phantom was used for the measurements in MRM1. The phantom has a diameter of 35 cm and a mass of 32 kg. It consists of 13 slices of tissue-equivalent material, composed of 8.6 % hydrogen, 2.6 % nitrogen, 32.3 % oxygen and 56.5 % carbon (by mass). Precise detector locations employed for the phantom measurements in MRM1 are discussed later in this article.

Table 2. Properties of the SBDS detectors used in this work.

Detector set	Detector number	Serial number	Detector type	S_{AmBe} (bubble mSv^{-1})
1	A91	1315	SBDS-10	145 ± 19
1	A92	1415	SBDS-100	153 ± 12
1	A93	1714	SBDS-600	139 ± 22
1	A94	1921	SBDS-1000	214 ± 83
1	A95	2112	SBDS-2500	121 ± 53
1	A96	2305	SBDS-10000	46 ± 3
2	A01	1216	SBDS-10	160 ± 37
2	A02	1514	SBDS-100	135 ± 9
2	A03	1614	SBDS-600	141 ± 18
2	A04	1823	SBDS-1000	227 ± 100
2	A05	2016	SBDS-2500	156 ± 80
2	A06	2205	SBDS-10000	46 ± 4

RESULTS AND DISCUSSION

Radi-N2 measurements in the USOS

Neutron energy spectra recorded by the SBDS in the four Radi-N2 sessions during ISS-34/35 (sessions A–D) are provided in Figure 1. The spectra were obtained by unfolding the bubble counts from the six SBDS detectors using the empirical response matrix described in Smith *et al.*[7]. As for the earlier ISS measurements, the spectrum-stripping technique[14] was used with non-negativity constraints. The data are provided as plots of $E\Phi(E)$ (in units of cm^{-2}) as a function of energy E, where Φ is the neutron fluence. In each of these plots, the solid line represents the fluence spectrum and the dashed and dotted lines represent the maximum and minimum fluence calculated from the data using the technique described in Smith *et al.*[7]. The dashed and dotted lines provide a measure of the positive and negative uncertainties.

The general features of the unfolded spectra are in agreement with previous measurements of the energy spectrum in space. The expected peaks at around 1 MeV and above 10 MeV are observed in the data from all four USOS locations. These characteristic

Table 3. Dates and locations of the experiments performed during this study.

Session	Initialisation date	Retrieval date	Location, SBDS 1	Location, SBDS 2
A	27 December 2012	3 January 2013	Columbus	Service module
B	18 January 2013	25 January 2013	JEM	Service module
C	11 February 2013	18 February 2013	US laboratory	Service module
D	5 March 2013	12 March 2013	Node 2	Service module
E	3 April 2013	10 April 2013	Service module	Service module
F	1 May 2013	8 May 2013	MRM1	MRM1
G	30 May 2013	6 June 2013	US laboratory	MRM1
H	27 June 2013	5 July 2013	US laboratory	MRM1
I	12 July 2013	19 July 2013	MRM1	MRM1
J	25 July 2013	2 August 2013	JEM	MRM1
K	23 August 2013	30 August 2013	JEM	MRM1
L	16 September 2013	23 September 2013	MRM1	MRM1
M	15 October 2013	22 October 2013	MRM1	MRM1

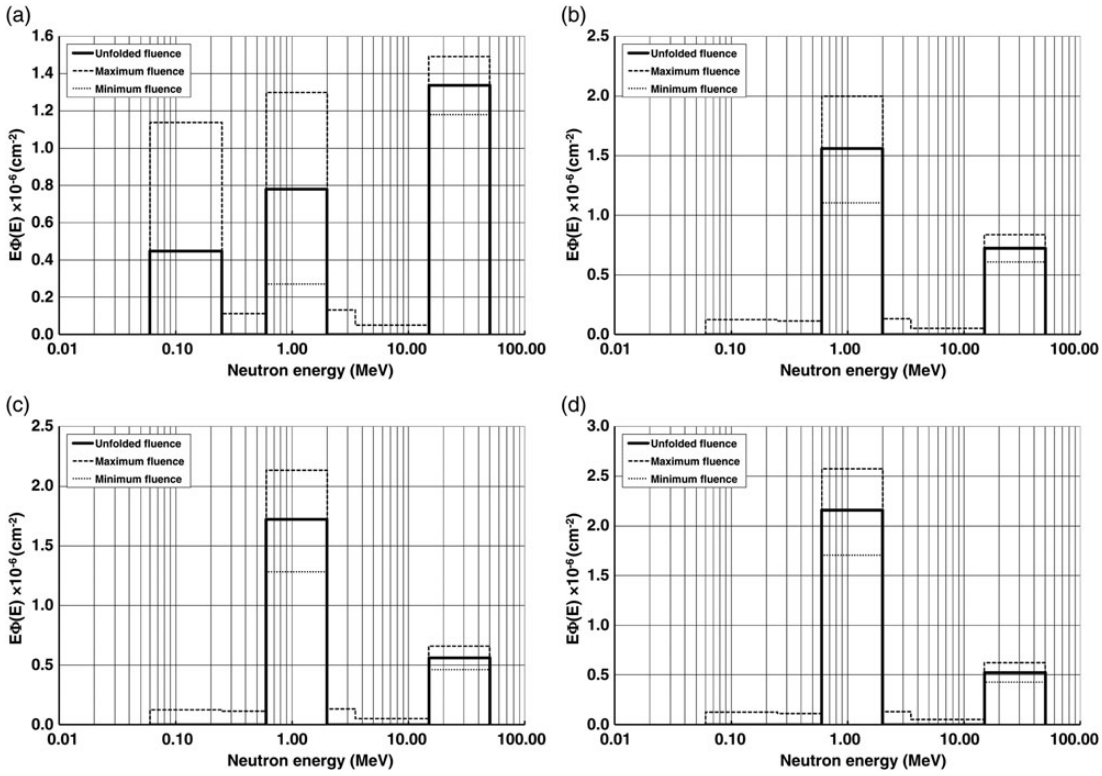

Figure 1. SBDS spectra collected from (**a**) session A in Columbus, (**b**) session B in the JEM, (**c**) session C in the US laboratory and (**d**) session D in Node 2.

features have been observed in earlier work using bubble detectors[3–5, 7, 8] and other instruments[11, 15] deployed in aircraft and spacecraft. The limited counting statistics of a single week-long measurement (discussed earlier in this article) are apparent in the data shown in Figure 1. For example, Figure 1a from the Columbus module includes an additional spectral peak at 100 keV. While this feature is potentially interesting, it is likely due to statistical fluctuations in the unfolding process. This feature will be investigated by combining these data with those from future measurements in Columbus.

Figure 2 presents the dose rate measured using the SBDS for the four Radi-N2 sessions during ISS-34/35, in comparison with the SBDS dose rate measured during the 2009 Radi-N experiment in the same locations. No corresponding measurement was made in Node 2 for the Radi-N experiment. For the other three locations, the agreement between the Radi-N and Radi-N2 measurements is excellent, with the Radi-N2 dose slightly higher than the Radi-N dose in all three locations.

Dose rates measured using the two SPNDs are presented in Figure 3. The data from the four Radi-N2

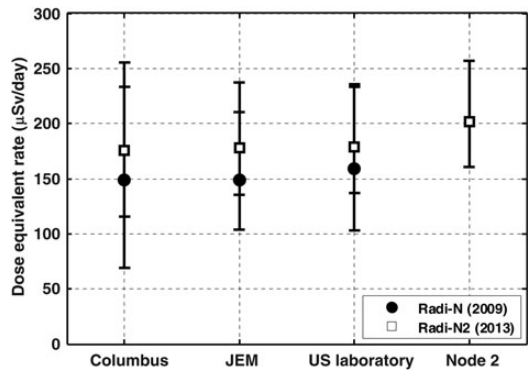

Figure 2. Comparison of dose rates measured with the SBDS for Radi-N and the Radi-N2 sessions performed during ISS-34/35.

sessions from ISS-34/35 (Figure 3b) are compared with the corresponding results[7] from ISS-20/21 (Figure 3a). In each panel of the figure, the dose rate measured by the detector worn on the astronaut's body

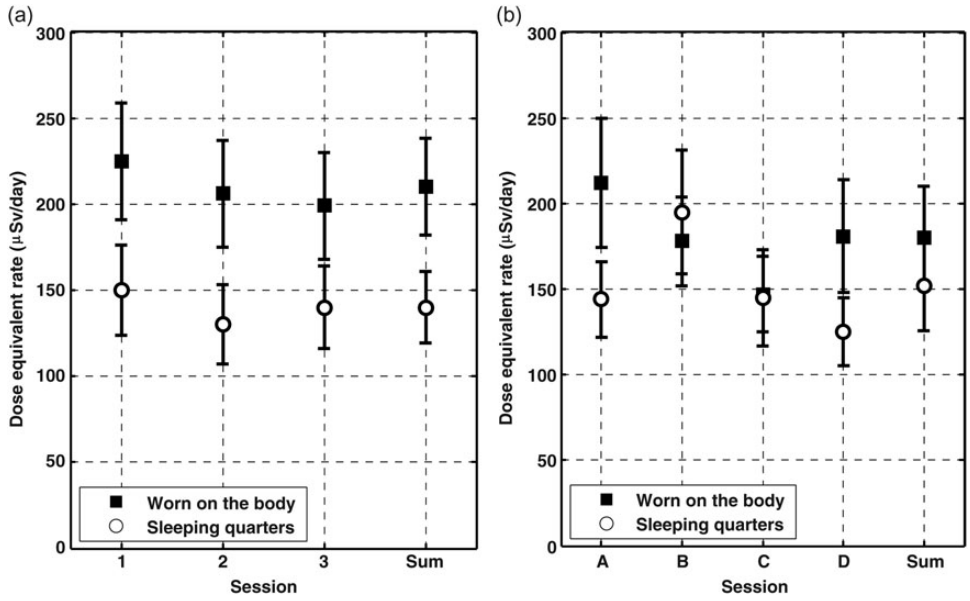

Figure 3. SPND dose rates for (**a**) Radi-N (2009) and (**b**) four Radi-N2 sessions during ISS-34/35 (2013).

is compared with that measured in the sleeping quarters. Data are presented for each session individually (sessions 1–3 from ISS-20/21 and A–D from ISS-34/35) and for the sum of all sessions from each expedition. The summed dose rate was determined by aggregating the bubble counts from the individual sessions, then calculating a dose rate from the summed counts. This provides an average value across the multiple measurements, with a smaller statistical uncertainty than for the dose rate from the individual sessions. For both Radi-N and Radi-N2, it is shown that the dose rate measured by the body-worn detector is higher than that measured in the sleeping quarters. This is possibly because the body-worn detector moved around the ISS, sampling higher dose rates in parts of the station in which the neutron flux was higher than in the sleeping quarters. The difference observed in 2009 was more pronounced than that measured in 2013. One important difference between the two measurements is the location of the sleeping quarters. In 2009, the astronauts slept in the JEM, whereas in 2013 the sleeping quarters were in Node 2.

Four more sessions were performed for the Radi-N2 experiment during ISS-35/36 using the same detectors (A91–A98) used for ISS-34/35. Two sessions were conducted in each of the US laboratory and the JEM, with the detectors placed in the same locations as for ISS-20/21 and ISS-34/35. An important difference between the Radi-N2 measurements performed during ISS-35/36 and the earlier Radi-N and Radi-N2 sessions was that the two SPNDs were not worn by an astronaut and left in the sleeping quarters during ISS-35/36. Instead, the two SPNDs were co-located with the SBDS.

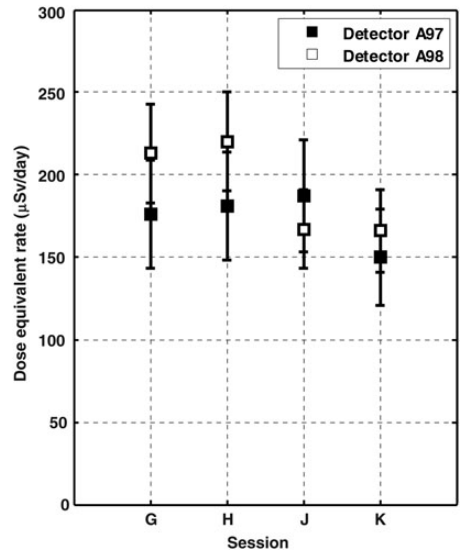

Figure 4. Dose rate measured using two SPNDs for four sessions in the USOS during ISS-35/36. Sessions G and H were conducted in the US laboratory, while sessions J and K were performed in the JEM.

Figure 4 presents the dose rate measured using two SPNDs for the four Radi-N2 sessions from ISS-35/36. Sessions G and H were performed in the US laboratory, while sessions J and K took place in the JEM.

Figure 5 shows the dose rate measured using the SBDS for these same sessions, as well as the earlier SBDS measurements from ISS-20/21 and ISS-34/35. The data from the JEM are presented in Figure 5a and those from the US laboratory are provided in Figure 5b. By the end of ISS-35/36, four sessions had been performed in each of the JEM and the US laboratory: one during ISS-20/21, one during ISS-34/35 and two during ISS-35/36. The SBDS dose rate is presented in Figure 5 for each of the four sessions in each location and for the aggregated data from those four sessions. Note that two sessions were performed in the JEM during ISS-20/21[7] but only the second of them is used in this comparison. This is because the SBDS was sandwiched between water shielding for the first ISS-20/21 session in the JEM, making those data difficult to compare with the other measurements. The SBDS data show good consistency for the four measurements in each of the two locations. Furthermore, the agreement between the SPND (Figure 4) and SBDS (Figure 5) is good. The data suggest that, at the time of these measurements, the neutron dose in the JEM and the US laboratory was very similar.

A summary of the dose rates measured using detector set 1, which includes all experiments in the USOS, is provided in Table 4. Detector set 1 was deployed in the USOS with the exception of sessions E, F, I, L and M, for which these detectors were used in the Russian segment. Table 4 includes the SPND and SBDS dose rates for each session, as well as the percentage of the SBDS dose due to neutrons above 15 MeV (i.e. those in the highest energy bin of the SBDS spectrum). The contribution of these high-energy neutrons is in good

Table 4. Summary of dose measurements using detector set 1.

Session	SBDS 1 dose rate (μSv d^{-1})	SBDS 1 dose >15 MeV (%)	A97 dose rate (μSv d^{-1})	A98 dose rate (μSv d^{-1})
A	176^{+79}_{-60}	62	212 ± 38	144 ± 22
B	178^{+59}_{-43}	35	195 ± 36	178 ± 26
C	179^{+57}_{-42}	28	145 ± 28	147 ± 22
D	202^{+55}_{-41}	22	181 ± 33	125 ± 20
E	159^{+62}_{-46}	57	192 ± 35	176 ± 25
F	121^{+63}_{-43}	65	151 ± 29	147 ± 22
G	181^{+64}_{-47}	53	176 ± 33	213 ± 30
H	163^{+58}_{-43}	58	181 ± 33	220 ± 30
I	139^{+61}_{-45}	64	142 ± 27	119 ± 19
J	144^{+57}_{-42}	63	187 ± 34	167 ± 24
K	126^{+59}_{-29}	88	150 ± 29	166 ± 25
L	136^{+63}_{-46}	67	99 ± 20	97 ± 16
M	117^{+38}_{-13}	100	142 ± 27	147 ± 22

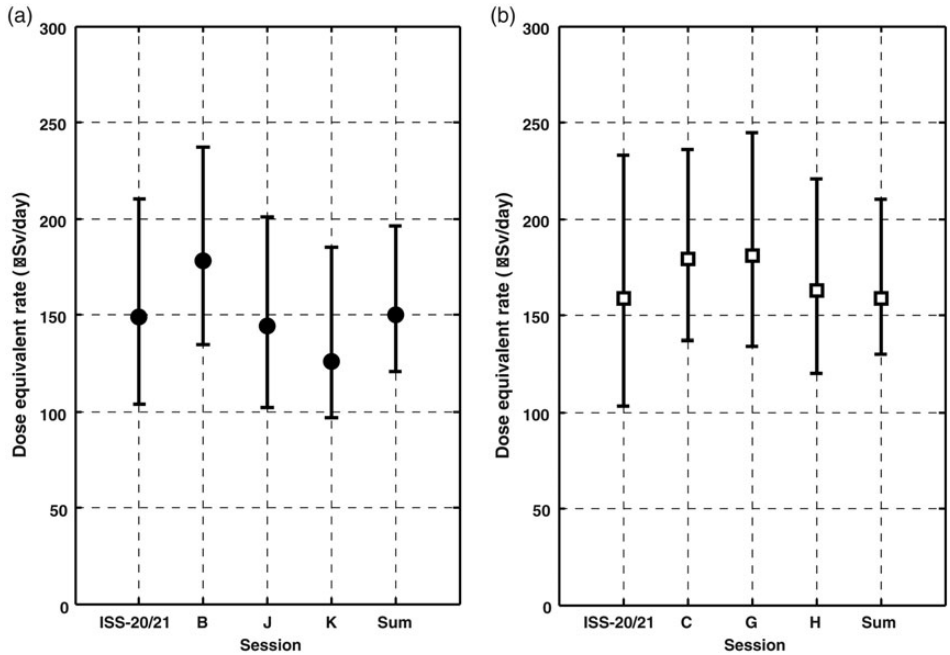

Figure 5. Dose rate measured during ISS-20/21, ISS-34/35 and ISS-35/36 using a SBDS in (**a**) the JEM and (**b**) the US laboratory.

agreement with the earlier bubble-detector measurements[3, 4, 7, 8] performed in LEO.

Comparison of the data from Radi-N and Radi-N2 (e.g. Figures 2, 3 and 5) suggests that the magnitude of the neutron dose was very similar in 2009 and 2013. This is perhaps surprising, given the large difference in solar activity between the two sets of measurements. The 2009 experiments took place at a time of low solar activity, whereas the Radi-N2 measurements were performed close to solar maximum. It is also worth noting that the ISS altitude was higher in 2013 than in 2009. Both the solar activity and the ISS altitude might be expected to influence the neutron dose inside the ISS.

The Wolf (sunspot) number, an indicator of solar activity, and the ISS altitude (apogee and perigee) are

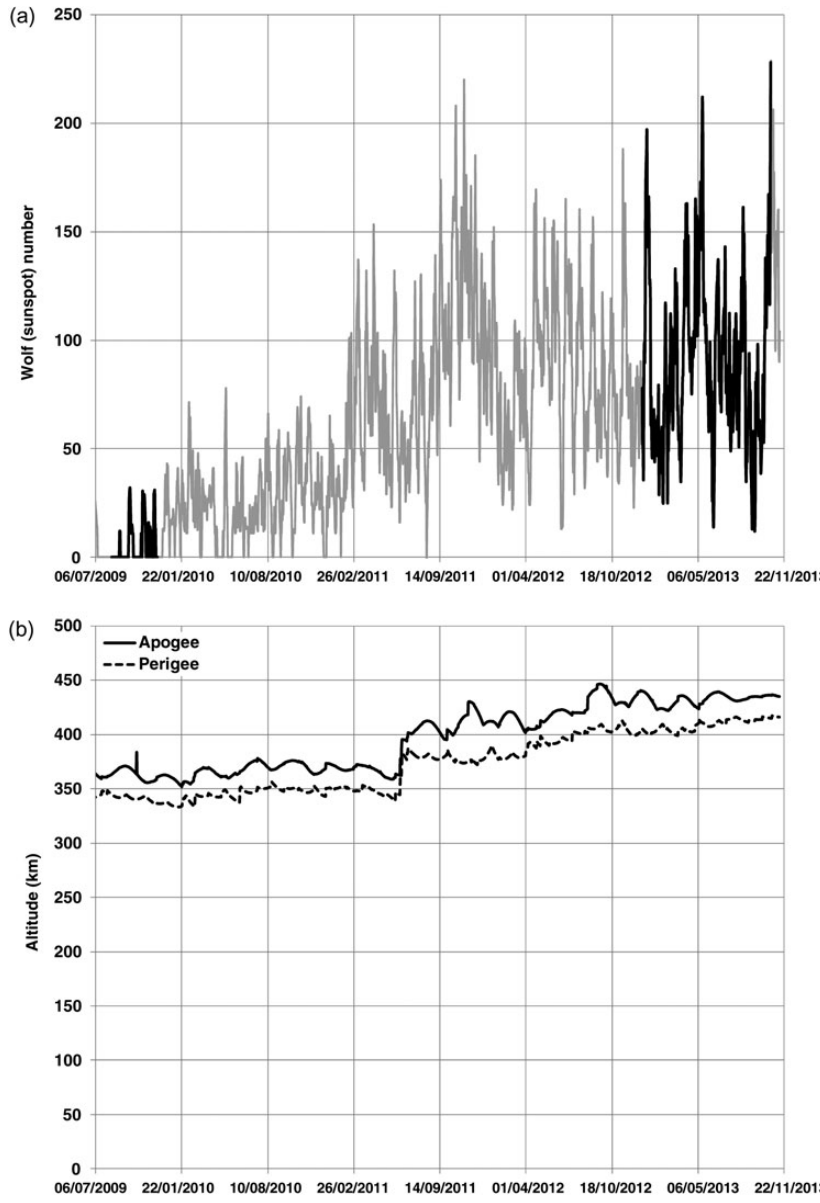

Figure 6. Plots of (**a**) Wolf number and (**b**) ISS altitude, measured from July 2009 to November 2013. The periods corresponding to the bubble-detector measurements during ISS-20/21 (2009) and ISS-34 to ISS-37 (2012–13) are indicated by the dark lines in panel (a).

presented in Figure 6 for the period from July 2009 to November 2013. The periods corresponding to the 2009 Radi-N experiments and the measurements described in this article are highlighted in Figure 6a. It is generally expected that solar activity will influence the overall radiation dose in space, with lower doses expected in LEO when the solar activity is high[16]. This is because matter emitted by the sun (primarily the plasma known as the solar wind) can reduce the magnetic rigidity of cosmic rays entering the Earth's magnetosphere. The diminished rigidity of incoming cosmic rays may in turn lead to a reduction in the dose due to trapped radiation in the Van Allen belts. Conversely, the overall radiation dose in LEO is expected to increase as the ISS altitude increases[16]. This is because, at higher altitudes, the ISS orbit is further into the Van Allen radiation belts where the flux of trapped protons is higher. The contribution of cosmic rays may also be larger at higher altitude. Given that variations in the solar activity or the orbital altitude can influence the charged particle flux incident on the ISS, these changes might also be expected to influence the flux of secondary neutrons inside the space station.

Based on the similarity in the Radi-N and Radi-N2 results, it appears that the differences in solar activity and ISS altitude between 2009 and 2013 did not have a strong effect on the neutron dose in the ISS. This observation agrees well with the earlier conclusions[8] from the Russian segment. In the study of Smith *et al.*[8], it was noted that the recent solar maximum may not have been strong enough to produce observable changes in the neutron field in the ISS. It was also noted that the effects of increased solar activity and increased altitude tend to cancel each other. These arguments may explain why the neutron dose seems constant as a function of time, in spite of the variations in potential influence quantities.

Matroshka-R experiments in the Russian segment

The Matroshka-R measurements described in this work were performed in two locations, namely the service module and MRM1. Table 5 provides dose-rate data obtained using detector set 2 in the Russian segment. For sessions E, F, I, L and M, detector set 1 was also deployed in the Russian segment, and dose information from those measurements is included in Table 4. SBDS dose data are not included in Table 5 for sessions F–K individually. For these measurements, which used the tissue-equivalent phantom in MRM1, the data were summed as described below. SBDS dose information for sessions L and M is also absent from Table 5 because of issues with some of the detectors (see below).

Experiments were conducted in the service module using detector set 2 for sessions A–D and using both detector sets for session E. For sessions A, B, D and E, all detectors were co-located on panel 327. For session C, an experiment was performed using the hydrogenous shield[8] studied during ISS-22 to ISS-33. The SBDS (A01–A06) was located in the right cabin of the service module, on the illuminator side of the hydrogenous shield. SPND A07 was located in the right cabin, on panel 443 (to the left of the protective shield), and SPND A08 was positioned on the cabin side of the hydrogenous shield.

Table 5. Summary of dose measurements using detector set 2.

Session	SBDS 2 dose rate (μSv d^{-1})	SBDS 2 dose >15 MeV (%)	A07 dose rate (μSv d^{-1})	A08 dose rate (μSv d^{-1})
A	144^{+75}_{-58}	61	151 ± 22	149 ± 24
B	228^{+45}_{-19}	100	150 ± 22	153 ± 25
C	126^{+58}_{-41}	49	148 ± 22	132 ± 22
D	154^{+41}_{-15}	100	187 ± 26	166 ± 26
E	162^{+62}_{-46}	55	172 ± 24	148 ± 24
F	n/a	n/a	90 ± 15	143 ± 23
G	n/a	n/a	140 ± 21	154 ± 25
H	n/a	n/a	140 ± 20	121 ± 20
I	n/a	n/a	160 ± 23	129 ± 21
J	n/a	n/a	131 ± 19	126 ± 20
K	n/a	n/a	193 ± 27	160 ± 26
L	n/a	n/a	154 ± 22	98 ± 17
M	n/a	n/a	177 ± 25	115 ± 20

The data for sessions F–K were aggregated as described in the text. For sessions L and M, the data for SBDS 2 were excluded from the data analysis because of detector issues.

The dose-rate measurements in the service module are summarised in Figure 7. The SBDS results (Figure 7a) include measurements using SBDS 2 for sessions A–D and both spectrometer sets for session E. The SBDS data show good consistency across the five sessions, although the dose rate measured for session B is higher than for the other sessions. The SPND dose rates for the same five sessions are plotted in Figure 7b. Two SPNDs were used for sessions A–D and four were used for session E. The SPND results show good consistency and agree well with the SBDS measurements. For session C, the detectors were placed on and around the hydrogenous shield, in order to assess the shielding effect of neutron radiation. Some effect of the shielding can be seen (Figure 7b) by the fact that the dose measured by SPND A08 (located on the hydrogenous shield) is lower than that measured by A07 on panel 443. The dose rate measured by the SBDS, which was also located on the protective shield, is also slightly lower for this session than for the other sessions. These results are consistent with the extensive study performed using this hydrogenous shield during ISS-22 to ISS-33[8].

The remaining measurements in the Russian segment were performed in MRM1 using the

spherical Matroshka-R phantom. The phantom measurements used detector set 2 (A01–A08) for all seven sessions and detector set 1 (A97–A98) for the three sessions that did not coincide with Radi-N2 measurements in the USOS. It was only possible to insert three bubble detectors into the phantom at any one time, so a single measurement using a complete SBDS in the phantom was not feasible. A plan was devised in which the detectors of SBDS 2 alternated between the phantom surface and the inside of the phantom, so that the aggregated data could be used to create spectra for the phantom surface and the inside of the phantom. Spectroscopic data were also collected above the phantom in three sessions using SBDS 1. The SPNDs were deployed above the phantom, at its surface, and inside the phantom. The locations of the detectors for the seven phantom sessions (sessions F–L) are provided in Tables 6 and 7. The phantom was located behind panel 206 of MRM1 for all seven sessions. Following the measurements with the phantom, both detector sets were deployed behind panel 206 without the phantom present for session M.

Towards the end of ISS-35/36, some of the bubble detectors began to reach the end of their useful life, which is typically 9 months. For some of the detectors, some number of bubbles could not be reliably recompressed following each measurement (according to information conveyed by the cosmonaut conducting the experiments) and it became difficult to interpret the detector data. Small numbers of bubbles were subtracted in the data analysis for some of these later sessions. For sessions L and M, the number of incompressible bubbles increased for some of the

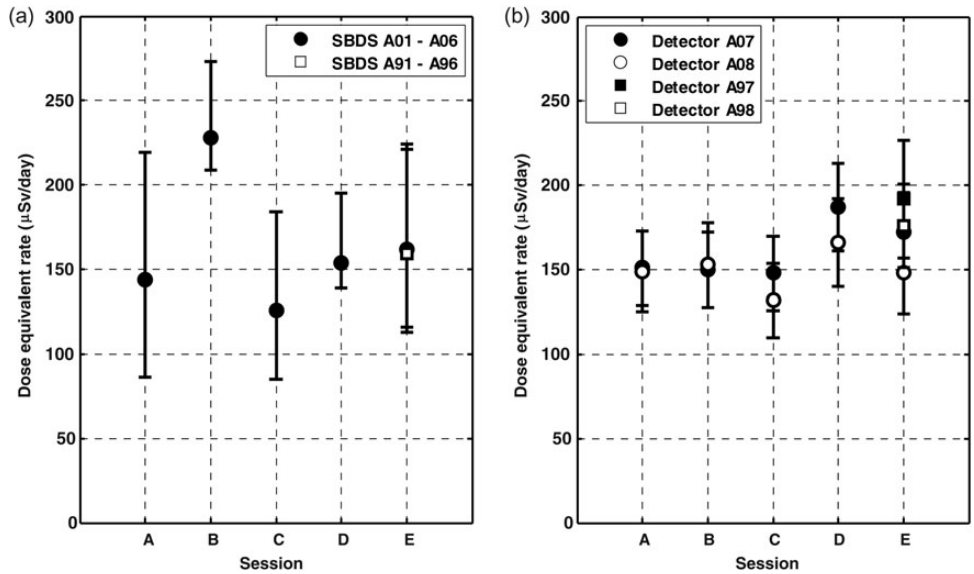

Figure 7. Dose rates measured in the Russian service module using (**a**) two bubble spectrometers and (**b**) four bubble dosemeters.

Table 6. Summary of positions for detector set 2 during the phantom measurements in MRM1.

Session	A01	A02	A03	A04	A05	A06	A07	A08
F	Inside phantom			Phantom surface			Inside phantom	Phantom surface
G	Inside phantom			Phantom surface			Phantom surface	
H	Phantom surface			Inside phantom			Phantom surface	
I	Inside phantom			Phantom surface			Inside phantom	Phantom surface
J	Inside phantom			Phantom surface			Phantom surface	
K	Phantom surface			Inside phantom			Phantom surface	
L	Phantom surface						Phantom surface	Inside phantom

detectors of SBDS 2. The results for SBDS 2 from these two sessions are considered to be unreliable and were therefore excluded from the analysis reported in this article.

The SBDS data were summed, using the information provided in Tables 6 and 7, to create aggregated neutron energy spectra for the surface of the phantom, the inside of the phantom and the location above the phantom. Figure 8 presents the spectrum measured on the phantom surface (Figure 8a) and the spectrum measured inside the phantom (Figure 8b). The dose information extracted from the unfolded SBDS data is provided in Table 8. The dose rate and the percentage of the dose due to neutrons above 15 MeV are provided for the spectra from the phantom surface, inside the phantom and above the phantom. The SBDS data suggest that the neutron dose inside the phantom is 66 % of the dose at its surface, while the dose above the phantom is very similar to that at the surface of the phantom. Figure 8 also illustrates that the energy spectrum inside the phantom appears to be different from that at the phantom surface and elsewhere in the ISS. The data suggest that neutrons inside the

Table 7. Summary of locations for detector set 1 during the phantom measurements.

Session	A91–A96	A97–A98
F	Above phantom	Above phantom
I	Above phantom	Above phantom
L	Above phantom	Inside phantom

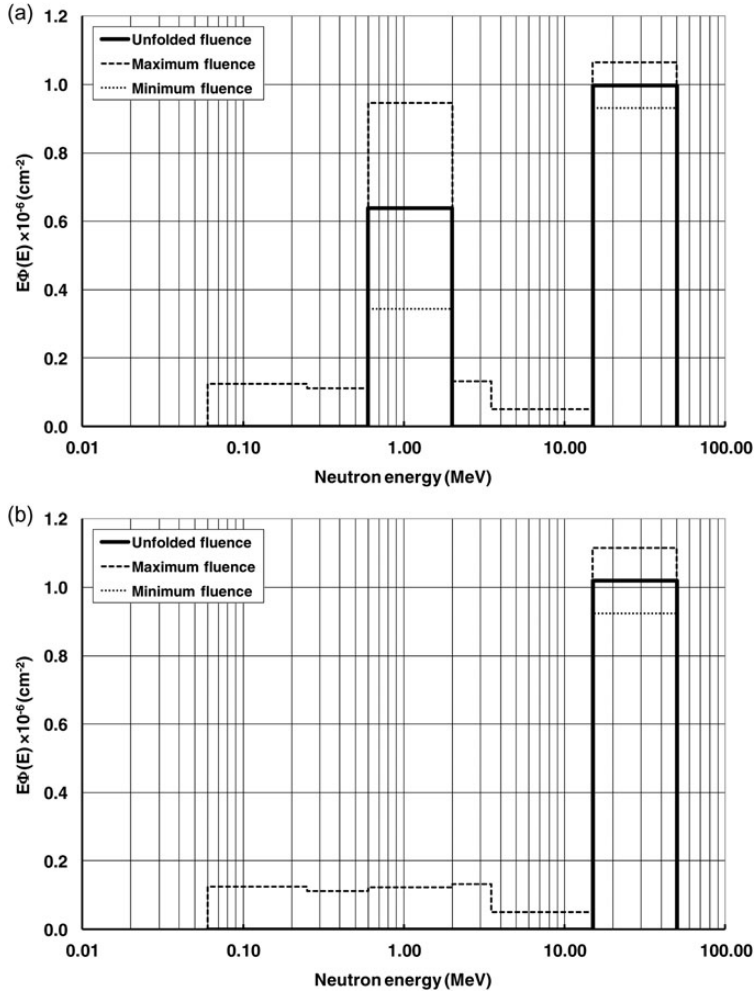

Figure 8. Unfolded neutron energy spectrum (**a**) on the phantom surface and (**b**) inside the phantom.

phantom have a higher average energy than neutrons outside the phantom, with all of the neutrons inside the phantom having energy above 15 MeV.

The SPND data from the seven phantom sessions were aggregated to obtain dose-rate values for the same three locations: at the phantom surface, inside the phantom and above the phantom. Dose-rate information measured by the SPNDs is presented in Table 8 and Figure 9. As for the SBDS, the SPND dose rates at the phantom surface and above the phantom are very similar. The SPND results suggest that the neutron dose inside the phantom is 73 ± 17 % of the dose at the phantom surface. This result agrees well with the value (i.e. 66 %) provided by the SBDS, and with the earlier SPND data[6] collected using the same phantom during ISS-13 to ISS-19, which suggested a similar dose reduction inside the phantom.

Table 8. Aggregated dose measurements using the Matroshka-R phantom.

Location	SBDS dose rate (μSv d^{-1})	SBDS dose >15 MeV (%)	SPND dose rate (μSv d^{-1})
Phantom surface	133^{+45}_{-27}	65	143 ± 23
Inside phantom	88^{+33}_{-8}	100	105 ± 18
Above phantom	135^{+47}_{-30}	65	140 ± 24

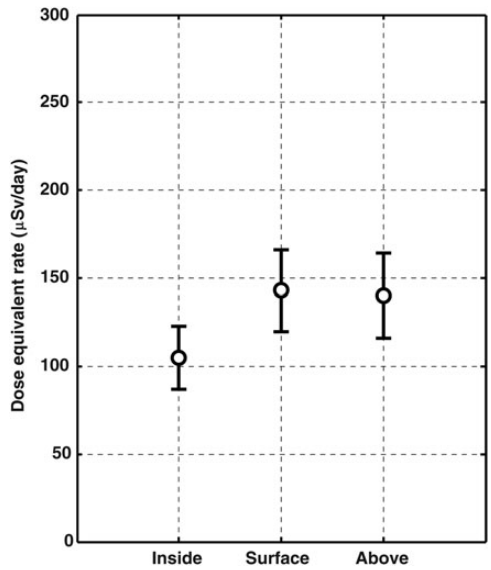

Figure 9. Comparison of SPND dose rates measured inside the Matroshka-R phantom, on its surface, and above the phantom.

The neutron dose rate measured inside the spherical phantom was 88 μSv d^{-1} using the SBDS and 105 μSv d^{-1} using the SPND. These values can be compared with the readings of a Liulin-5 silicon telescope, which was also located inside the phantom at the time of the bubble-detector experiments. This device[17, 18] has been used to measure the radiation dose inside the Matroshka-R phantom over an extended period of time. At the time of the bubble-detector measurements in the phantom, the Liulin-5 recorded typical values of 140 μGy d^{-1} for absorbed dose and 390 μSv d^{-1} for dose equivalent. As expected, the dose equivalent recorded by the Liulin-5 is higher than that measured by the bubble detectors. This is because the Liulin-5 is sensitive to particles with a wide range of linear energy transfer (LET), while the bubble detector only measures high-LET particles[2, 13].

A possible explanation for the shape of the neutron spectrum inside the phantom is that the tissue-equivalent material attenuates neutrons entering the phantom, while high-energy secondary neutrons are created by reactions of charged particles in the phantom. This hypothesis has been tested using Monte Carlo simulations to investigate the reactions of neutrons and charged particles in the phantom. The simulations were performed using the Geant4 software toolkit[19] (version 10.0, patch 1). The Geant4 physics list, which defines the processes included in the simulations, was the same as that used for recent investigations of the bubble-detector response to neutrons[13]. This custom physics list was based on Geant4's built-in QBBC list with a small number of modifications. NeutronHP physics was added for neutrons with energy below 20 MeV; standard electromagnetic (EM) physics was replaced with Penelope EM physics; and neutron tracking cuts were disabled.

The phantom was modelled as a sphere of tissue-equivalent material, using the dimensions and material composition given earlier in this article. The hollow centre of the sphere, with radius of 5 cm, was included in the model but the radial holes that accommodate the detectors were not modelled. Parallel beams of neutrons, protons and alpha particles were fired at the surface of the phantom. Heavier charged particles were not considered in the simulations. For each incoming particle type, an input energy spectrum was used that represents the field inside the ISS. These spectra were calculated in earlier work[7, 10] by transporting particles through aluminium shielding chosen to represent the shell of the ISS. The input spectra of neutrons and protons were taken from Armstrong and Colborn[10] and were computed by transporting the relevant particles through reduced-density aluminium shielding with areal density of 20.7 g cm^{-2}. The input alpha-particle spectrum was calculated in Smith *et al.*[7] using the CREME96 (Cosmic Ray Effects on Micro-Electronics, 1996 revision) code[20]. For these calculations, the aluminium shielding in the model had areal density of 8 g cm^{-2}.

The input spectra incident on the phantom surface and the calculated neutron spectra inside the phantom are shown in Figure 10. The data are presented in the form of $E\Phi(E)$ as a function of energy to enable comparison with the spectra measured using the SBDS. Figure 10a provides the input spectra used for neutrons, protons and alpha particles. Figure 10b presents the results of the simulations, showing the spectrum of neutrons created by incoming neutrons, protons and alpha particles. The simulations suggest that most of the neutrons inside the phantom are due to incoming neutrons that scatter in the tissue-equivalent material, while incident protons and alpha particles also create neutrons via (p, n) and (alpha, n) reactions in the phantom. The low yield of neutrons due to alpha particles suggests that heavier charged particles (which are less abundant than alpha particles) do not contribute significantly to the neutron field in the phantom.

The theoretical neutron spectra presented in Figure 10 exhibit the same qualitative features as the spectra recorded using the SBDS (Figure 8). The simulated data reproduce the empirically measured observation that the neutron spectrum in the phantom is harder than that outside the phantom. This supports the idea that the phantom attenuates incident neutrons, while charged particles create high-energy secondary neutrons inside the phantom. It is also apparent from Figure 10b that thermal neutrons (with energy around 10^{-8} MeV) are also produced in the phantom. It would therefore be expected that these low-energy neutrons are also created in the tissue of ISS crewmembers. While these thermal neutrons are abundant in the phantom, their contribution to the total dose received is low. Based on the spectra shown in Figure 10b, the thermal neutron contribution is <4 % of the total neutron dose inside the phantom. It is worth noting that the bubble detectors used in this work are not sensitive to thermal neutrons, so this contribution is absent from the experimental spectra presented in Figure 8.

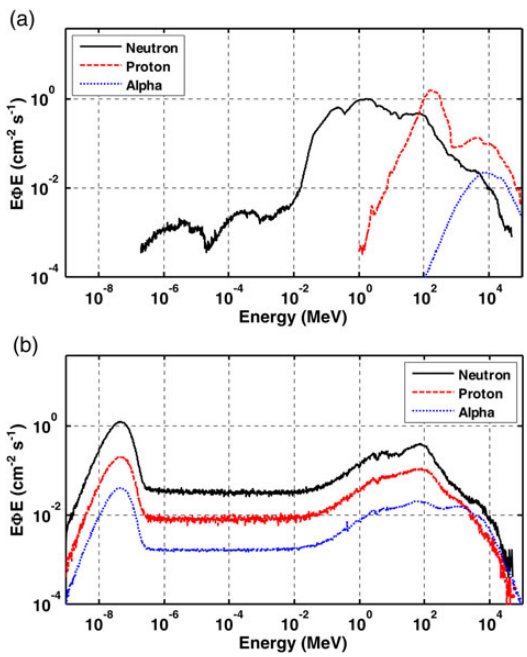

Figure 10. (**a**) The neutron, proton and alpha-particle energy spectra used as input for the Monte Carlo simulations, involving the Matroshka-R phantom. (**b**) The neutron spectra inside the phantom resulting from incident neutrons, protons and alpha particles.

Dose-rate information was determined from the input neutron spectrum and the spectra calculated inside the phantom, enabling a comparison with the dose rates measured by the bubble detectors. For neutron energies below 20 MeV, dose conversion factors were taken from Report 74 of the International Commission on Radiological Protection (ICRP-74). This report provides factors that convert neutron fluence to ambient dose equivalent, $H^*(10)$. For energies of 20 MeV and above, the dose conversion factors given in Sannikov and Savitskaya[21] were used. The dose rate determined from the input neutron spectrum incident on the phantom is 157 μSv d^{-1}, which agrees well with the measurements at the phantom surface and above the phantom (Table 8). The simulated neutron spectra inside the phantom yield dose rates of 65 μSv d^{-1} from incoming neutrons, 20 μSv d^{-1} due to neutrons created by incoming protons and 6 μSv d^{-1} from neutrons produced by incident alpha particles. The total neutron dose calculated inside the phantom is therefore 91 μSv d^{-1}, which is in good agreement with the SBDS and SPND dose rates measured in the phantom (presented in Table 8).

CONCLUSIONS

A large volume of information regarding the neutron dose and energy spectrum inside the ISS has been collected using bubble detectors. A series of measurements was performed between December 2012 and October 2013 for the Radi-N2 and Matroshka-R experiments. For Radi-N2, measurements were conducted in four modules of the USOS: Columbus, the JEM, the US laboratory and Node 2. The Radi-N2 results are not significantly different from the Radi-N data from the same ISS locations in 2009, despite the changes in solar activity and ISS altitude that have occurred since the earlier measurements. This conclusion agrees with that of earlier experiments in the Russian segment, suggesting that these potential influence quantities have little effect on the neutron field in the ISS. For Matroshka-R, experiments using a second set of detectors in the Russian segment included the first determination of the neutron spectrum in and around

the spherical Matroshka-R phantom. These measurements suggest that the neutron dose inside the phantom is ~70 % of the dose at the phantom surface. It is also shown that the spectrum inside the phantom contains a larger fraction of high-energy neutrons than the spectrum outside the phantom. The results of the phantom experiments agree well with Monte Carlo simulations performed using the Geant4 software.

ACKNOWLEDGEMENTS

The authors would like to thank the astronauts and cosmonauts who performed the experiments described in this work. NASA's Space Radiation Analysis Group (SRAG) is gratefully acknowledged for its support of the measurements. The authors would also like to thank Jordanka Semkova for providing the Liulin-5 data discussed in this article.

FUNDING

This work was supported by the Canadian Space Agency and the Russian Space Agency.

REFERENCES

1. Ing, H. and Mortimer, A. *Space radiation dosimetry using bubble detectors*. Adv. Space Res. **14**(10), 73–76 (1994).
2. Ing, H., McLean, T. D., Noulty, R. A. and Mortimer, A. *Bubble detectors and the assessment of biological risk from space radiations*. Radiat. Prot. Dosim. **65**(1–4), 421–424 (1996).
3. Ing, H., Noulty, R. A. and McLean, T. D. *Bubble detectors: a maturing technology*. Radiat. Meas. **27**(1), 1–11 (1997).
4. Ing, H. *Neutron measurements using bubble detectors–terrestrial and space*. Radiat. Meas. **33**, 275–286 (2001).
5. Lewis, B. J. *et al*. *Review of bubble detector response characteristics and results from space*. Radiat. Prot. Dosim. **150**(1), 1–21 (2012).
6. Machrafi, R. *et al*. *Neutron dose study with bubble detectors aboard the International Space Station as part of the Matroshka-R experiment*. Radiat. Prot. Dosim. **133**(4), 200–207 (2009).
7. Smith, M. B. *et al*. *Measurements of the neutron dose and energy spectrum on the International Space Station during expeditions ISS-16 to ISS-21*. Radiat. Prot. Dosim. **153**(4), 509–533 (2013).
8. Smith, M. B., Khulapko, S., Andrews, H. R., Arkhangelsky, V., Ing, H., Lewis, B. J., Machrafi, R., Nikolaev, I. and Shurshakov, V. *Bubble-detector measurements in the Russian segment of the International Space Station during 2009–12*. Radiat. Prot. Dosim. **163**(1), 1–13 (2015).
9. Badhwar, G. D. (ed). *Recommendations of the predictions and measurements of secondary neutrons in space workshop*, NASA/Johnson Space Center, September 28–30, 1998. Published in part in *Radiat. Meas.* **33** (2001).
10. Armstrong, T. W. and Colborn, B. L. *Predictions of secondary neutrons and their importance to radiation effects inside the international space station*. Radiat. Meas. **33**(3), 229–234 (2001).
11. Green, A. R., Andrews, H. R., Bennett, L. G. I., Clifford, E. T. H., Ing, H., Jonkmans, G., Lewis, B. J., Noulty, R. A. and Ough, E. A. *Bubble detector characterization for space radiation*. Acta Astronaut. **56**, 949–960 (2005).
12. Green, A. R., Bennett, L. G. I., Lewis, B. J., Tume, P., Andrews, H. R., Noulty, R. A. and Ing, H. *Characterisation of bubble detectors for aircrew and space radiation exposure*. Radiat. Prot. Dosim. **120**(1–4), 485–490 (2006).
13. Smith, M. B., Andrews, H. R., Ing, H. and Koslowsky, M. R. *Response of the bubble detector to neutrons of various energies*. Radiat. Prot. Dosim. **164**(3), 203–209 (2015).
14. Knoll, G. F. *Radiation Detection and Measurement*, 3rd edn. Wiley (2000). ISBN 0 471 07338 5.
15. Goldhagen, P., Reginatto, M., Kniss, T., Wilson, J. W., Singleterry, R. C., Jones, I. W. and Van Steveninck, W. *Measurement of the energy spectrum of cosmic-ray induced neutrons aboard an ER-2 high-altitude airplane*. Nucl. Instrum. Meth. Phys. Res. A **476**, 42–51 (2002).
16. Durante, M. and Cucinotta, F. A. *Physical basis of radiation protection in space travel*. Rev. Mod. Phys. **83**(4), 1245–1281 (2011).
17. Semkova, J. *et al*. *Radiation measurements inside a human phantom aboard the International Space Station using Liulin-5 charged particle telescope*. Adv. Space Res. **45**, 858–865 (2010).
18. Semkova, J., Dachev, T., Koleva, R., Bankov, N., Maltchev, St., Benghin, V., Shurshakov, V. and Petrov, V. *Observation of radiation environment in the International Space Station in 2012–March 2013 by Liulin-5 particle telescope*. J. Space Weather Space Clim. **4**, A32 (2014).
19. Agostinelli, S. *et al*. *Geant4–a simulation toolkit*. Nucl. Instrum. Meth. Phys. Res. A **506**(3), 250–303 (2003); http://geant4.web.cern.ch/.
20. Tylka, A. J., Adams, J. H. Jr, Boberg, P. R., Brownstein, B., Dietrich, W. F., Flueckiger, E. O., Petersen, E. L., Shea, M. A., Smart, D. F. and Smith, E. C. *CREME96: a revision of the cosmic ray effects on micro-electronics code*. IEEE Trans. Nucl. Sci. **44**(6), 2150–2160 (1997); https://creme.isde.vanderbilt.edu/.
21. Sannikov, A. V. and Savitskaya, E. N. *Ambient dose equivalent conversion factors for high energy neutrons based on the ICRP 60 recommendations*. Radiat. Prot. Dosim. **70**(1–4), 383–386 (1997).